



## **COMPRESSIBILITY EFFECTS ON HYPERSONIC BLUNT BODY SHOCK STANDOFF**

**Wilson F. N. Santos**

[Wilson@lcp.inpe.br](mailto:Wilson@lcp.inpe.br)

Combustion and Propulsion Laboratory  
National Institute for Space Research  
Cachoeira Paulista, SP 12630-000

***Abstract.** Computations using the Direct Simulation Monte Carlo (DSMC) method are presented for hypersonic flow over flat-nose leading edges. The primary aim of this paper is to examine the effect of the compressibility on the shock-wave structure. The sensitivity of shock-wave shape, shock standoff distance, and shock thickness to freestream Mach number variations is calculated by using a model that classifies the molecules in three distinct classes: (1) undisturbed freestream, (2) reflected from the boundary and (3) scattered, i.e., molecules that had been indirectly affected by the presence of the leading edge. The analysis shows significant differences on the shock-wave structure due to variations on the freestream Mach number from 5 to 12. It was found that the flat-nose leading edges provided smaller shock-wave standoff distance and shock-wave thickness, compared to a reference circular cylinder that generated the flat-nose bodies.*

**Keywords:** DSMC, Hypersonic Flow, Rarefied Flow, Blunt Body, Shock Standoff.

### **1. INTRODUCTION**

It is well known that a shock wave is produced when a supersonic/hypersonic flow impinges upon a stationary body. If the body has a blunt nose or a sharp nose with a quite large nose angle, the shock wave is curved and lies upstream of the body. Acknowledge of shock-wave structure around hypersonic blunt bodies is of interest for many reasons. Among them, to estimate shock wave interference effects on winged- or finned-body missile configurations, to calculate re-entry body convective heating in the presence of large inviscid shock-layer entropy gradients, and to predict radiative heat transfer from high-temperature shock layers around manned superorbital re-entry vehicles. Such knowledge can be obtained from detailed numerical blunt body flowfield analysis that gives solutions for the shock-wave structure, such as the shock-wave shape, shock-wave detachment distance and shock-wave thickness.

The successful design of high-lift, low-drag hypersonic configurations will depend on the ability to incorporate relatively sharp leading edges that combine good aerodynamic properties with acceptable heating rates. Certain hypersonic configurations, such as waveriders (Nonweiler, 1959), are designed analytically with infinitely sharp leading edge for shock-wave attachment. Nevertheless, for practical applications, these sharp leading edges must be blunted for heat transfer, manufacturing, and handling concerns, with associated departures from ideal performance. Typically, a round leading edge with constant radius of curvature near the stagnation point has been chosen. Nonetheless, shock detachment distance on a cylinder, with associated leakage, scales with the radius of curvature. In this connection, certain classes of non-circular shapes may provide the required bluntness with smaller shock separation than round leading edges, thus allowing manufacturing, and fundamentally heating control, with reduced aerodynamic losses.

The idea that such non-circular shapes would be possible is based on the work of Reller (1957) who has presented a method of designing low heat transfer bodies. The method is devised on the premise that the rate of heat transfer to the nose will be low if the local velocity is low, while the rate of heat transfer to the afterbody will be low if the local density is low. A typical body that results from this design method consists of a flat nose followed by a highly curved, but for the most part slightly inclined, afterbody surface.

Santos (2003) has investigated the effect of the leading edge thickness on the aerodynamic surface quantities over these flat-nose leading edges. The thickness effect was examined for a range of Knudsen number, based on the thickness of the flat face, covering from the transitional flow regime to the free molecular flow regime. The emphasis of the work was to compare the heat flux and drag of this new shape with those obtained for round leading edge. Santos (2004) has extended the analysis presented by Santos (2003) by investigating computationally the shock-wave structure over these new contours. The primary goal was to assess the sensitivity of the shock standoff distance, shock-wave thickness and shock-wave shape to variations not only on the flat-face thickness but also on the body surface temperature. Santos (2005a) has further extended the investigation presented by Santos (2003) by examining the gas-surface interaction effects on the flowfield structure.

In continuation of the research on flat-nose leading edges, the present account extends the analysis presented by Santos (2003, 2004 and 2005a) by examining computationally the shock structure on these blunt leading edges with a great deal of emphasis placed on the compressibility effects. The flow conditions represent those experienced by a spacecraft at altitude of 70 km. Therefore, the focus of the present study is the low-density region in the upper atmosphere, where numerical gaskinetic procedures are available to simulate hypersonic flows. High-speed flows under low-density conditions deviate from a perfect gas behavior because of the excitation of the internal modes of energy. At high altitudes, and therefore low density, the molecular collision rate is low and the energy exchange occurs under non-equilibrium conditions. In such a circumstance, the degree of molecular non-equilibrium is such that the Navier-Stokes equations are inappropriate. In the current study, the DSMC method is used to examine the shock structure for the idealized situation of rarefied hypersonic two-dimensional flow. Attention will be addressed to the analysis of the shape, thickness and position of the shock wave relative to the body producing it.

## 2. BODY-SHAPE DEFINITION

The geometry of the leading edges considered in this work is the same as that presented in Santos (2003). The blunt shapes consist of a flat nose supplemented by an afterbody surface defined, in dimensionless form, by the following contour,

$$\bar{x} = \int_{\bar{y}=1}^{\bar{y}=\bar{y}_{\max}} \sqrt{\bar{y}^k - 1} d\bar{y} \quad \text{where } \bar{x} = x/y_{\text{nose}} \text{ and } \bar{y} = y/y_{\text{nose}} . \quad (1)$$

The blunt shapes are modeled by assuming a sharp leading edge of half angle  $\theta$  with a circular cylinder of radius  $R$  inscribed tangent to the wedge. The blunt shapes are inscribed tangent to them at the same common point where they have the same slope angle. It was assumed a leading edge half angle of 10 degrees, a circular cylinder diameter of  $10^{-2}$ m and flat-face thickness  $t/\lambda_{\infty}$  of 0.01, 0.1 and 1, where  $t = 2y_{\text{nose}}$  and  $\lambda_{\infty}$  is the freestream mean free path. Figure (1a) illustrates this construction for the set of shapes investigated. From geometric considerations, the exponent  $k$  in Eq. (1) is obtained by matching slope on the wedge, circular cylinder and on the body shapes at the tangency point. For dimensionless thicknesses of 0.01, 0.1 and 1, the exponent  $k$  corresponds to 0.501, 0.746 and 1.465, respectively. The common body height  $H$  and the body length  $L$  are obtained in a straightforward manner. It was assumed that the leading edges are infinitely long but only the length  $L$  is considered, since the wake region behind the leading edges is not of interest in this investigation.

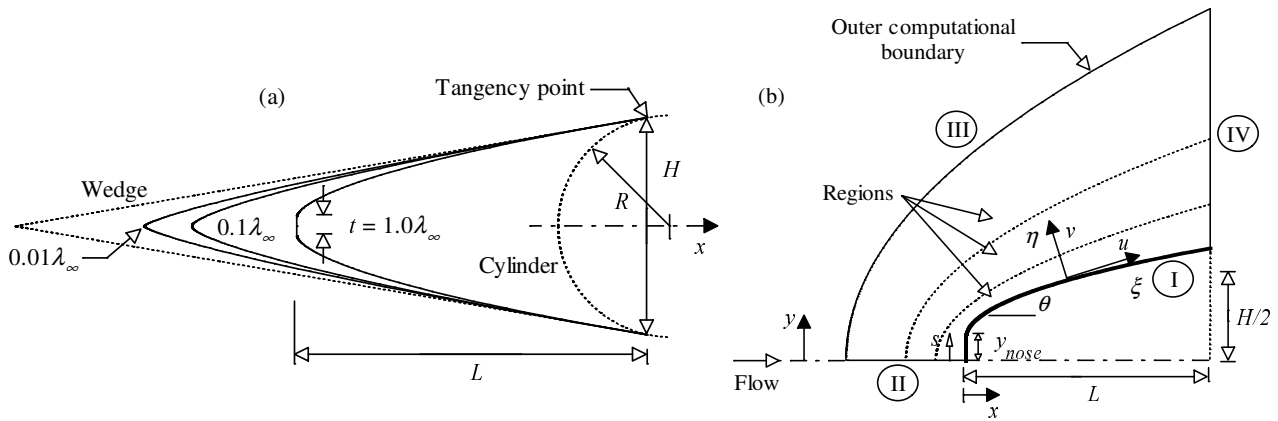


Figure 1: Drawing illustrating (a) the leading edge shapes and (b) the computational domain.

### 3. COMPUTATIONAL METHOD

The most successful numerical technique for modeling complex flows in the transitional regime has been the Direct Simulation Monte Carlo (DSMC) method developed by Bird (1994). DSMC models the flow as being a collection of discrete particles, each one with a position, velocity and internal energy. The state of the particles is stored and modified with time as the particles move, collide, and undergo boundary interactions in simulated physical space.

In this study, collisions are modeled by using the variable hard sphere (VHS) molecular model (Bird, 1981) and the no time counter (NTC) collision sampling technique (Bird, 1989). Repartition energy among internal and translational modes is controlled by the Borgnakke-Larsen statistical model (Borgnakke and Larsen, 1975). Simulations are performed using a non-reacting gas model for a constant freestream gas consisting of 76.3% of  $N_2$  and 23.7% of  $O_2$ . Energy exchanges between translational and internal modes, rotational and vibrational, are considered. Relaxation collision numbers of 5 and 50 were used for the calculations of rotation and vibration, respectively.

In the DSMC method, the physical space is divided into a certain number of cells and each cell is also divided into subcells. The physical space network is used to facilitate the choice of molecules for collisions and for the sampling of the macroscopic flow properties such as temperature, pressure, etc. In the DSMC algorithm, the linear dimensions of the cells should be small in comparison with the scale length of the macroscopic flow gradients normal to streamwise directions, which means that the cell dimensions should be of the order of or smaller than the local mean free path (Bird, 1994).

The computational domain used for the calculation is made large enough so that body disturbances do not reach the upstream and side boundaries, where freestream conditions are specified. A schematic view of the computational domain is depicted in Fig. (1b). Side I is defined by the body surface. Diffuse reflection model is the condition applied to this side. Advantage of the flow symmetry is taken into account, and molecular simulation is applied to one-half of a full configuration. Thus, side II is a plane of symmetry. In such a boundary, all flow gradients normal to the plane are zero. At the molecular level, this plane is equivalent to a specular reflecting boundary. Side III is the freestream side through which simulated molecules enter and exit. Finally, the flow at the downstream outflow boundary, side IV, is predominantly supersonic and vacuum condition is specified (Bird, 1994). At this boundary, simulated molecules can only exit.

The numerical accuracy in DSMC method depends on the cell size chosen, on the time step as well as on the number of particles per computational cell. These effects were investigated in order to determine the number of cells and the number of particles required to achieve grid independence solutions. Grid independence was tested by running the calculations with half and twice the number of cells in  $\xi$  and  $\eta$  directions (see Fig. 1(b)) compared to a standard grid. Solutions (not shown) were near identical for all grids used and were considered fully grid independent.

#### 4. FREESTREAM CONDITIONS

The freestream and flow conditions used in the present calculations are those given by Santos (2003) and summarized in Tab. (1). The gas properties considered in the simulation are those given by Bird (1994) and shown in Tab. (2). Referring to Tabs. (1) and (2),  $T_\infty$ ,  $p_\infty$ ,  $\rho_\infty$ ,  $n_\infty$ ,  $\mu_\infty$ , and  $\lambda_\infty$  stand respectively for temperature, pressure, density, number density, viscosity and mean free path, and  $X$ ,  $m$ ,  $d$  and  $\omega$  account respectively for mole fraction, molecular mass, molecular diameter and viscosity index.

Table 1: Freestream Conditions

| $T_\infty$ (K) | $p_\infty$ (N/m <sup>2</sup> ) | $\rho_\infty$ (kg/m <sup>3</sup> ) | $n_\infty$ (m <sup>-3</sup> ) | $\mu_\infty$ (Ns/m <sup>2</sup> ) | $\lambda_\infty$ (m)  |
|----------------|--------------------------------|------------------------------------|-------------------------------|-----------------------------------|-----------------------|
| 220.0          | 5.582                          | $8.753 \times 10^{-5}$             | $1.8209 \times 10^{21}$       | $1.455 \times 10^{-5}$            | $9.03 \times 10^{-4}$ |

Table 2: Gas Properties

|                | $X$   | $m$ (kg)                | $d$ (m)                | $\omega$ |
|----------------|-------|-------------------------|------------------------|----------|
| O <sub>2</sub> | 0.237 | $5.312 \times 10^{-26}$ | $4.01 \times 10^{-10}$ | 0.77     |
| N <sub>2</sub> | 0.763 | $4.650 \times 10^{-26}$ | $4.11 \times 10^{-10}$ | 0.74     |

The overall Knudsen number  $Kn_t$ , defined as the ratio of the freestream mean free path  $\lambda_\infty$  to the leading edge thickness  $t$ , corresponds to 100, 10 and 1 for leading edge thickness  $t/\lambda_\infty$  of 0.01, 0.1 and 1, respectively. The Reynolds number  $Re_t$  covers the range from 0.193 to 19.3, based on conditions in the undisturbed stream with the flat-face thickness  $t$  as the characteristic length. The wall temperature  $T_w$  on the body surface is maintained constant at 880 K for all cases considered.

In order to simulate the compressibility effect, the DSMC calculations were performed independently for three distinct numerical values for the freestream Mach number  $M_\infty$ , i.e., 5, 8 and 12. These values correspond to freestream velocity  $V_\infty$ , of 1.49, 2.37 and 3.56 km/s.

#### 4. COMPUTATIONAL PROCEDURE

The problem of predicting the shock-wave displacement is especially important in a waverider geometry (Nonweiler, 1959), since these hypersonic configurations usually rely on shock-wave attachment at the leading edge to achieve their high lift-to-drag ratio at high-lift coefficient.

In this present account, the shock-wave structure, defined by shape, thickness and detachment of the shock wave, is predicted by employing a procedure based on the physics of the particles. In this scenario, the flow is assumed to consist of three distinct classes of molecules; those molecules from the freestream that have not been affected by the presence of the leading edge are denoted as class I molecules; those molecules that, at some time in their past history, have struck and been reflected from the body surface are denoted as class II molecules; and finally, those molecules that have been indirectly affected by the presence of the body are defined as class III molecules. Figure (2a) illustrates the definition for the molecular classes.

Based on this classification, it is assumed that the class I molecule changes to class III molecule when it collides with class II or class III molecule. Class I or class III molecule is progressively transformed into class II molecule when it interacts with the body surface. Also, a class II molecule remains class II regardless of subsequent collisions and interactions. As a result, the transition from class I molecules to class III molecules may represent the shock wave, and the transition from class III to class II may define the boundary layer.

A typical distribution of class III molecules along the stagnation streamline for blunt leading edges is illustrated in Fig. (2b) along with the definition used to determine the thickness, displacement and shape of the shock wave. In this figure,  $X$  is the distance  $x$  along the stagnation

streamline (see Fig. (1b)), normalized by the freestream mean free path  $\lambda_\infty$ , and  $f_{III}$  is the number of molecules for class III to the total amount of molecules inside each cell.

Referring to Fig. (2b), the shock standoff distance  $\Delta$  is defined as being the distance between the shock-wave center and the nose of the leading edge along the stagnation streamline. Therefore, the center of the shock wave is defined by the station that corresponds to the maximum value for  $f_{III}$ . The shock-wave thickness  $\delta$  is defined by the distance between the stations that correspond to the mean value for  $f_{III}$ . Finally, the shock-wave shape (shock wave “location”) is determined by the coordinate points given by the maximum value in the  $f_{III}$  distribution along the lines departing from the body surface, i.e.,  $\eta$ -direction as shown in Fig. (1b).

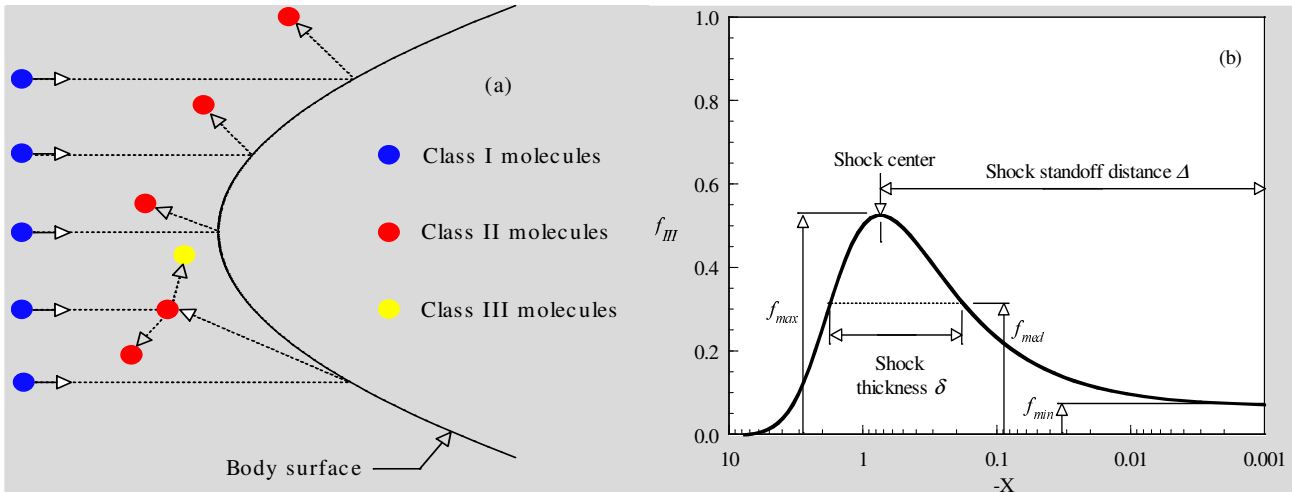


Figure 2: (a) Drawing illustrating the molecule classification and (b) Schematic of shock structure.

## 5. COMPUTATIONAL RESULTS AND DISCUSSION

The purpose of this section is to discuss and to compare differences in the shape, thickness and displacement of the shock wave due to variations on the freestream Mach number as well as on the leading edge thickness. Before proceeding with the analysis of the shock-wave structure, it is desirable to highlight the major features of the results related to the molecular class distribution.

### 5.1. Molecular Class Distribution

The distribution of molecules for classes I, II and III along the stagnation streamline is illustrated in Figs. (3) and (4) for four cases that combine two different nose thicknesses,  $Kn_t$  of 100 and 1 ( $t/\lambda_\infty$  of 0.01 and 1), and freestream Mach number of 5 and 12. The class distributions for the other cases investigated in this work are intermediate to these four cases and, therefore, they will not be shown.

According to Figs. (3) and (4),  $f_I$ ,  $f_{II}$  and  $f_{III}$  are the ratio of the number of molecules for class I, II and III, respectively, to the total amount of molecules inside each cell along the stagnation streamline. In this set of plots, particular attention is paid to the behavior of the class I molecules for the bodies representing sharp and blunt leading edges. It may be recognized that molecules from freestream, represented by class I molecules, collide with the nose of the leading edges even after the establishment of the steady state. This is shown in Fig. (3), which represents a sharp leading edge case. In contrast, molecules from freestream do not reach the nose of the leading edge for those cases illustrated in Fig. (4), which represent blunt leading edges. This is explained by the fact that density (Santos, 2006) increases much more for blunt (flat) leading edges in the stagnation region and reaches its maximum value in the stagnation point. Consequently, the buildup of particle density near the nose of the leading edge acts as a shield for the molecules coming from the undisturbed stream.

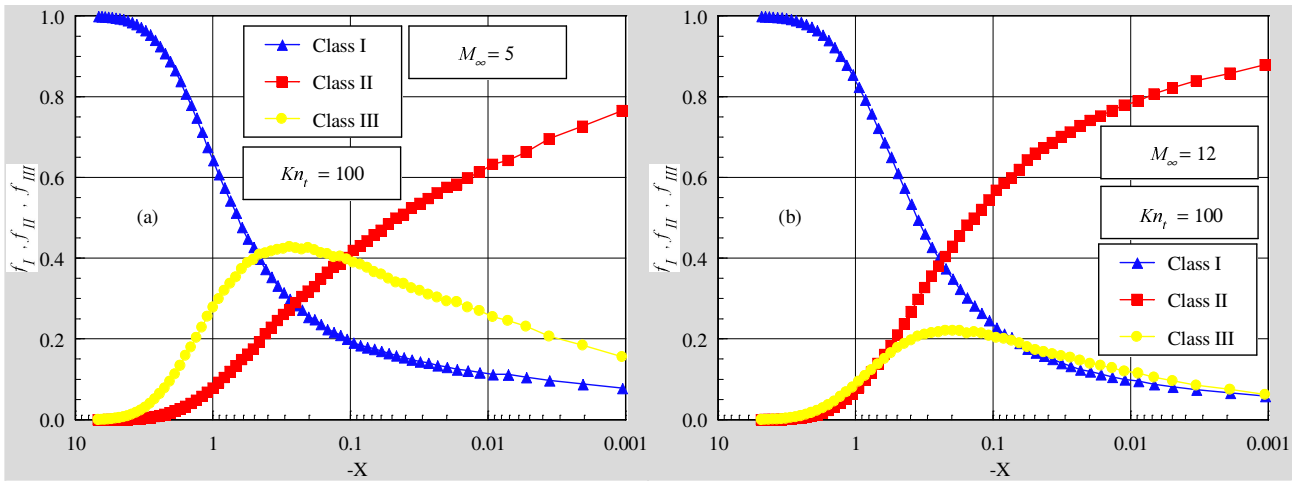


Figure 3: Distributions of molecules for classes I, II and III along the stagnation streamline for thickness Knudsen number  $Kn_t$  of 100 and freestream Mach number of (a) 5 and (b) 12.

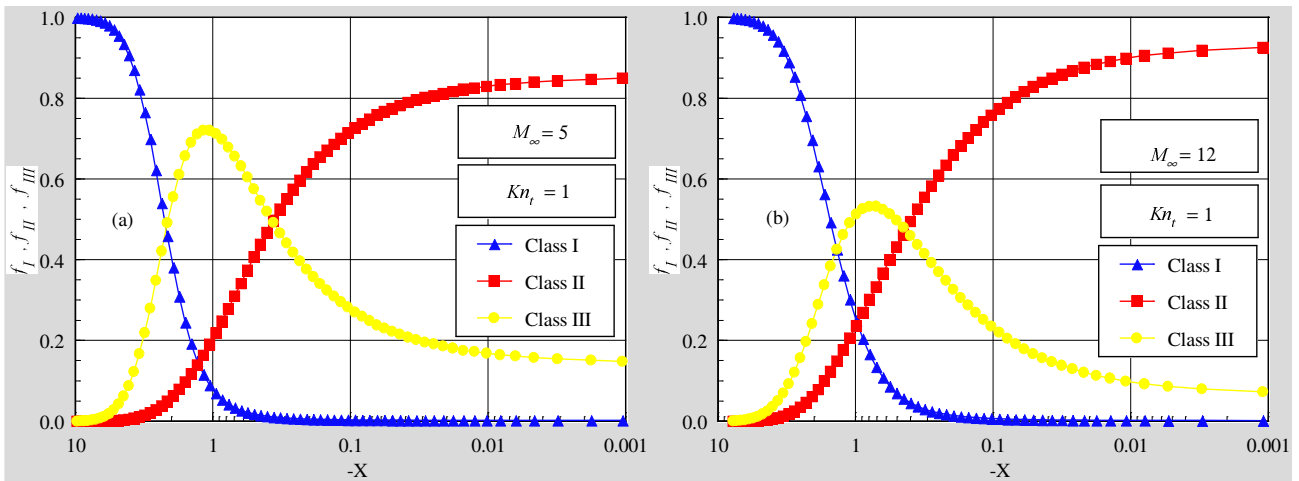


Figure 4: Distributions of molecules for classes I, II and III along the stagnation streamline for thickness Knudsen number  $Kn_t$  of 1 and freestream Mach number of (a) 5 and (b) 12.

### 5.2. Shock-Wave Standoff Distance

The shock standoff distance  $\Delta$  can be observed in Figs. (3) and (4) for the flat-nose leading edges shown. The calculated shock standoff distance  $\Delta$ , normalized by the freestream mean free path  $\lambda_\infty$  is tabulated in Tab. (3) for the cases investigated. It is apparent from these results that there is a discrete shock standoff distance for the cases shown. As would be expected, the shock standoff distance increases with increasing the flat-nose thickness. Moreover, the shock standoff distance decreases with the freestream Mach number rise. As a reference, for freestream Mach number of 5, the shock standoff distance for cases  $Kn_t$  of 100, 10 and 1 is around 1.3, 1.4 and 1.46 times, respectively, larger than those for freestream Mach number of 12.

According to Santos (2005b), the reference circular cylinder shown in Fig. (1a) provides a larger shock detachment, i.e.,  $\Delta/\lambda_\infty$  of 1.645 for freestream Mach number of 12. For comparison purpose, this value is about 8.2, 4.8 and 2.2 times larger than the cases corresponding to  $Kn_t$  of 100, 10 and 1, respectively, for the same freestream Mach number. The results tend to confirm the expectation that the shock standoff distance for sharp leading edge is smaller than that for blunt leading edge. In fact, the flat-nose bodies behave as if they had a sharper profile than the representative circular cylinder.

Table 3: Dimensionless shock-wave standoff distance  $\Delta/\lambda_\infty$  for flat-nose leading edges.

| $M_\infty$ | $Kn_t = 100$ | $Kn_t = 10$ | $Kn_t = 1$ |
|------------|--------------|-------------|------------|
| 5          | 0.260        | 0.481       | 1.096      |
| 8          | 0.226        | 0.373       | 0.842      |
| 12         | 0.201        | 0.346       | 0.753      |

It should be emphasized that shock standoff distance becomes important in hypersonic vehicles such as waveriders, which depend on leading edge shock attachment to achieve their high lift-to-drag ratio at high lift coefficient. In this connection, the flat-nose shapes seem to be more appropriate than the round leading edge (circular cylinder), since they present reduced shock wave detachment distances. Nonetheless, smaller shock detachment distance is associated with a higher heat load to the nose of the body. According to Santos (2003), the heat transfer coefficient  $C_{ho}$  ( $= 2q_w/\rho_\infty V_\infty^2$ ) at the stagnation point for flat-nose bodies,  $Kn_t$  of 100, 10 and 1, with freestream Mach number of 12, are 2.4, 2.2 and 1.5 times larger than the heat transfer coefficient for the circular cylinder (Santos, 2005b) at the same conditions. As a result, it should be notice from this comparison that the ideal blunting leading edge depends on the context. If shock standoff distance is the primary issue in leading edge design of hypersonic waveriders, then flat-nose leading edges are superior to round leading edges (circular cylinder). Contrary, if the stagnation point heating is the important parameter in the hypersonic vehicle design, then round shapes seem to be superior to the flat-nose shapes.

### 5.3. Shock-Wave Thickness

In conformity with the definition for shock-wave thickness shown in Fig. (2b), it proves useful to calculate the shock-wave thickness  $\delta$  along the stagnation streamline for the flat-nose shapes from Figs. (3) and (4). As a result of the calculation, Table (4) tabulates the shock-wave thickness  $\delta$ , normalized by the freestream mean free path  $\lambda_\infty$ , for the cases investigated.

Table 4: Dimensionless shock-wave thickness  $\delta/\lambda_\infty$  for flat-nose leading edges.

| $M_\infty$ | $Kn_t = 100$ | $Kn_t = 10$ | $Kn_t = 1$ |
|------------|--------------|-------------|------------|
| 5          | 0.922        | 1.191       | 2.051      |
| 8          | 0.722        | 0.949       | 1.735      |
| 12         | 0.652        | 0.864       | 1.673      |

Similar to the shock standoff distance, the shock thickness increases with increasing the flat-nose thickness and decreases with increasing the freestream Mach number. As a reference, for freestream Mach number of 5, the shock thickness for cases  $Kn_t$  of 100, 10 and 1 is around 1.4, 1.38 and 1.22 times, respectively, larger than those for freestream Mach number of 12.

For comparison purpose, the circular cylinder provides a much larger shock thickness, i.e.,  $\delta/\lambda_\infty$  of 3.350 for freestream Mach number of 12. Again, compared to the flat-nose shapes, this value is about 5.3, 3.9 and 2.0 times larger than the cases corresponding to  $Kn_t$  of 100, 10 and 1, respectively, for freestream Mach number of 12.

### 5.4. Shock-Wave Shape

The shock-wave shape, defined by the shock-wave center location, is obtained by calculating the position that corresponds to the maximum  $f$  for class III molecules in the  $\eta$ -direction along the afterbody surface. Figure (5) illustrates the shock-wave shape at the vicinity of the stagnation region

for cases  $Kn_t$  of 100 and 1, which correspond to flat-nose bodies with thicknesses  $t/\lambda_\infty$  of 0.01 and 1, respectively. The shock-wave shapes for  $Kn_t$  of 10 are intermediate to the cases depicted in Fig. (5) and they will not be shown. In this set of plots,  $X$  and  $Y$  are the Cartesian coordinates  $x$  and  $y$  normalized by  $\lambda_\infty$ .

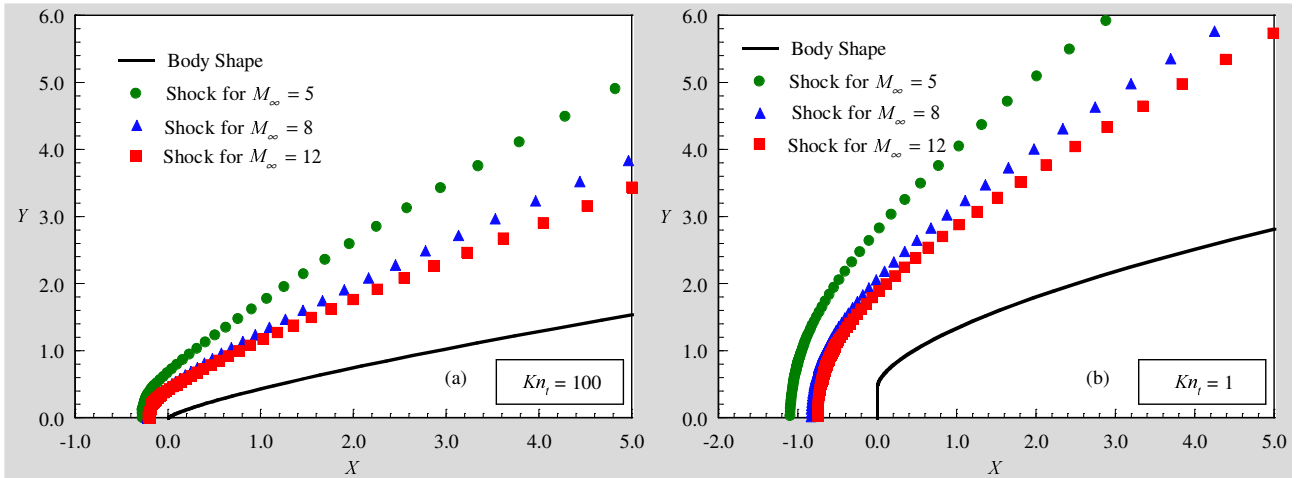


Figure 5: Shock wave shapes on flat-nose bodies as a function of the freestream Mach number for leading edge thickness corresponding to Knudsen number  $Kn_t$  of (a) 100 and (b) 1.

It was pointed out by Lees and Kubota (1957) that when the freestream Mach number  $M_\infty$  is sufficiently large, the hypersonic small-disturbance equations admit similarity solutions for the asymptotic shock-wave shapes over power-law bodies ( $y \propto x^n$ ,  $0 < n < 1$ ), where asymptotic refers to the flowfield at large distances downstream of the nose of the body. The hypersonic small-disturbance theory states that, for certain exponent  $n$ , a body defined by  $x^n$  produces a shock wave of similar shape and profiles of flow properties transverse to the stream direction that are similar at any axial station not too near the nose. At or near the nose, the surface slope, the curvature, and the higher derivatives are infinite, and the similarity solutions break down. In the more general case for  $0 < n < 1$ , the shock wave grows as  $x^m$ . When  $n$  grows from zero,  $m$  begins by keeping the constant value  $m = 2/(j+3)$ , and if  $n$  keeps on growing towards unity,  $m$  remains equal to  $n$ . Here  $j$  takes the values zero for planar flow and one for axisymmetric flow.

The flat-nose bodies, defined by Eq.(1), are not power-law shapes themselves, by they can be closely fitted with power-law shapes ( $\propto x^n$ ) far from the nose of the leading edge. Figure (6a) displays the comparison of the flat-nose shapes and the corresponding power-law curve fit shapes. As would be expected, discrepancies have been found among the curves at the vicinity of the nose of the bodies. This behavior is brought out more clearly in Fig. (6b), which exhibits details of the curves near the nose.

By considering the reference system located at the nose of the leading edges,  $X = 0$ , the fitting process, which has been performed over those bodies shown in Fig. (6), approximates the body shapes by power-law shapes of the following form,

$$y = a(x + b)^n \tag{2}$$

where  $a$  is the power-law constant of the curve fit,  $b$  is the distance from the nose of the leading edge, and  $n$  is the power-law exponent of the curve fit. The coefficients  $a$  and  $b$ , normalized, respectively, by  $\lambda_\infty^{(1-n)}$  and  $\lambda_\infty$ , and the exponent  $n$  are tabulated in Tab. (5). The maximum absolute error between the original shapes and the curve fit shapes for  $X > 3$  are less than 0.12%, 0.14% and 0.30% for flat-nose thicknesses corresponding to  $Kn_t$  of 100, 10 and 1, respectively.

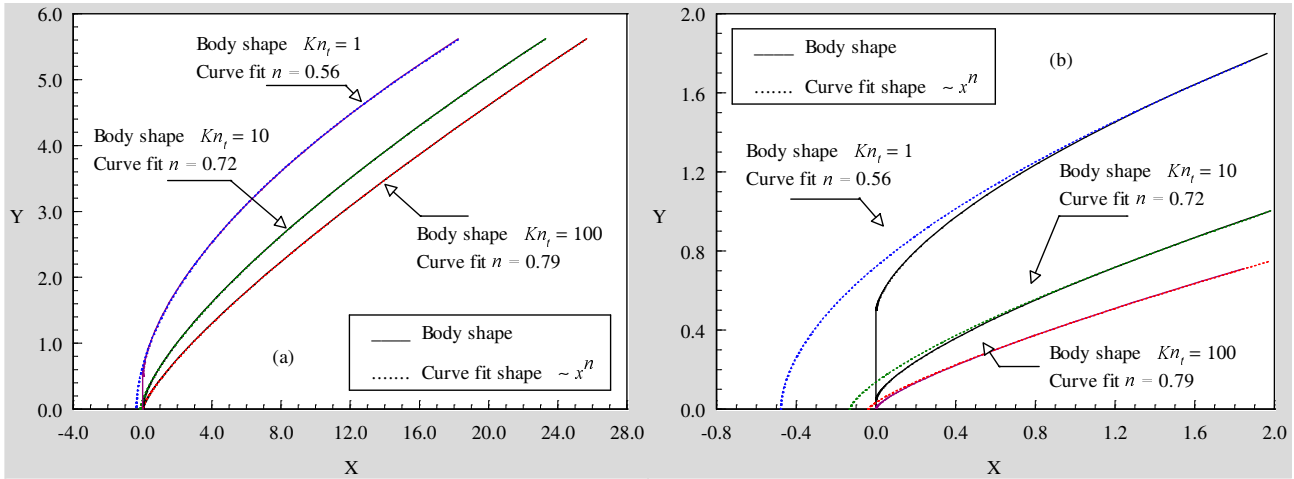


Figure 6: Comparison of flat-nose shapes with power-law curve fit shapes for leading edge thicknesses  $t/\lambda_\infty$  of 0.01, 0.1 and 1, which correspond to Knudsen number  $Kn_t$ , 100, 10 and 1. (a) along the afterbody surface and (b) at the vicinity of the nose.

Table 5: Dimensionless coefficients  $a$ ,  $b$ , and  $n$  for the curve fit power-law bodies.

| $Kn_t$ | $a$     | $b$     | $n$  |
|--------|---------|---------|------|
| 100    | 0.42893 | 0.04120 | 0.79 |
| 10     | 0.58436 | 0.13318 | 0.72 |
| 1      | 1.09002 | 0.47817 | 0.56 |

In what follows, the flat-nose leading edges shown in Fig. (6) are now well represented by shapes with the power-law form ( $\propto x^n$ ) far from the nose of the leading edges. Hence, by assuming that power-law bodies generate power-law shock waves in accordance with hypersonic small-disturbance theory (Lees and Kubota, 1957), the coordinate points for the shock location shown in Fig. (5) were used to approximate the shape of the shock wave with a curve fit. A fitting algorithm was performed over these points to approximate the shock shape as a power-law curve of the following form,

$$y = A(x + B)^m \tag{3}$$

where  $A$  is the shock-wave power-law constant,  $B$  is the distance from the nose of the leading edge to the shock-wave curve fit along the stagnation streamline, and  $m$  is the shock-wave power-law exponent.

For comparison purpose, two forms of the curve fit were considered in defining the shock shape: (1)  $A$ ,  $B$  and  $m$  were found to provide the best curve fit solutions, and (2)  $A$  and  $B$  were found by keeping  $m = 2/3$  for  $n < 2/3$  cases, and  $m = n$  for  $n \geq 2/3$  cases, where  $n$  and  $m$  stand for body and shock-wave power-law exponents, respectively.

It is worthwhile mentioning that the fitting process was performed over the points yielded by DSMC simulations located far from the nose region, say  $X > 3.0$ , where it is expected that the blunt nose effects are not significant. It is also important to recall that the shock-wave shape at the vicinity of the nose is not correctly predicted by the theoretical solutions, since the hypersonic slender body approximations are violated close to or at the nose of the leading edges as explained above. Moreover, the flat-nose shapes are represented by power-law shapes far from the nose region, as displayed in Fig. (6).

Curve fit solutions for shock shape over the flat-nose body with  $Kn_t$  of 100 ( $t/\lambda_\infty = 0.01$ ), which corresponds to a body power law exponent of 0.79, are displayed in Fig. (7a) for freestream Mach

number of 5. According to this figure, the solutions given by  $m = 0.78$  and  $m = n = 0.79$  represent, respectively, the two forms of the curve fit solutions mentioned above. It is apparent from this figure that the curve fit solutions present a good agreement, by visual inspection, with those solutions provided by the DSMC simulation. Nevertheless, as the maximum absolute error between the DSMC solutions and the curve fit solutions are calculated for coordinate points located at  $X > 3.0$ , it is found that the curve fit obtained by the first form of the fitting process presents slightly a better fit, i.e., when  $A$ ,  $B$  and  $m$  were found in order to yield the best solution. The error is less than 1.0% for the curves shown in Fig. (7a). In general, the solutions are in qualitative agreement with the Lees and Kubota (1957) findings in the sense that the shock-wave shape would follow the shape of the body for body power-law exponent  $n > 2/3$ .

Shock shape curve fit solutions for the flat-nose body with  $Kn_t$  of 1 ( $t/\lambda_\infty = 1$ ), which corresponds to a body power-law exponent of 0.56, are displayed in Fig. (7b) for freestream Mach numbers of 5. The curve fit solutions shown in this set of figures were obtained according to Eq.(3) by three different forms; in the first form,  $A$  and  $B$  were found by keeping  $m$  equal to the body shape,  $m = n$ ; in the second form,  $A$ ,  $B$  and  $m$  were found in order to obtain the best fit; finally in the third form,  $A$  and  $B$  were found by keeping  $m$  equal to  $2/3$ , the exponent that it is expected that the shock wave would grow, according to the theory (Lees and Kubota, 1957).

Referring to Fig. (7b), it is noted that the curve fit given by  $m = n = 0.56$  does not match the shock wave shape obtained by the DSMC simulation, as predicted by the hypersonic small-disturbance theory (Lees and Kubota, 1957). In contrast, the two other curve-fit solutions,  $m$  equal to  $2/3$  and  $0.668$  present an excellent agreement with those solutions provided by the DSMC simulation. Once again, the curve-fitted solution deviates from the DSMC solution close to the nose of the leading edge, as would be expected.

At this point, it should be emphasized that the curve fit exponents are very sensitive to the number of coordinate points, which define the shock wave, used in the fitting process. In addition, these coordinate points present fluctuations, originated from the DSMC simulations.

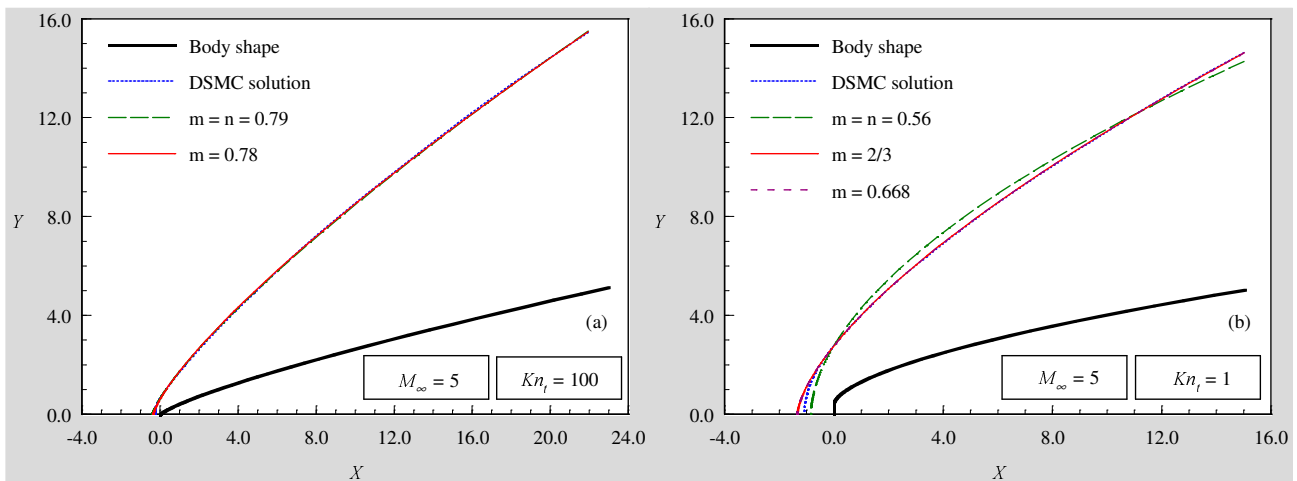


Figure 7: Shock wave shape curve fits on flat-nose bodies corresponding to thickness Knudsen number  $Kn_t$  of (a) 100 and (b) 1 for freestream Mach number of 5.

## 6. CONCLUDING REMARKS

This study applies the Direct Simulation Monte Carlo method to investigate the shock wave structure for a family of flat-nose leading edges. The calculations have provided information concerning the nature of the shock-wave detachment distance, shock-wave thickness and shock-wave shape resulting from variations not only on the flat-face thickness of the leading edges but also on the freestream Mach number for the idealized situation of two-dimensional hypersonic rarefied flow. The emphasis of the investigation was also to compare these flat-nose leading edges

with round shape (circular cylinder) in order to determine which geometry is better suited as a blunting profile in terms of the shock wave standoff distance.

The analysis showed that the shock-wave structure was affected by changes in the freestream Mach number. As expected, it was found that the shock wave standoff and the shock-wave thickness decrease with the freestream Mach number rise for the conditions investigated. In addition, the shock-wave was displaced further upstream the nose of the leading edges with decreasing the freestream Mach number. It was also found that the shock wave standoff distance and the shock wave thickness for the flat-nose bodies are lower than that for the circular body with the same tangency to a wedge of specified oblique angle. In addition, the computational results indicated that the shock-wave shape grows with power law form ( $\propto x^m$ ), for the flat-nose bodies investigated, which can be closely fitted with power-law shapes ( $\propto x^n$ ).

## 7. REFERENCES

- Bird, G. A., 1981, "Monte Carlo Simulation in an Engineering Context", Progress in Astronautics and Aeronautics: Rarefied gas Dynamics, Ed. Sam S. Fisher, Vol. 74, part I, AIAA New York, pp. 239-255.
- Bird, G. A., 1989, "Perception of Numerical Method in Rarefied Gasdynamics", Rarefied gas Dynamics: Theoretical and Computational Techniques, Eds. E. P. Muntz, and D. P. Weaver and D. H. Capbell, Vol. 118, Progress in Astronautics and Aeronautics, AIAA, New York, pp. 374-395.
- Bird, G. A., 1994, "Molecular Gas Dynamics and the Direct Simulation of Gas Flows", Oxford University Press, Oxford, England, UK.
- Borgnakke, C. and Larsen, P. S., 1975, "Statistical Collision Model for Monte Carlo Simulation of Polyatomic Gas Mixture", Journal of computational Physics, Vol. 18, No. 4, pp. 405-420.
- Lees, L. and Kubota, T., 1957, "Inviscid Hypersonic Flow over Blunt-Nosed Slender Bodies", Journal of Aeronautical Sciences, Vol. 24, No. 3, pp. 195-202.
- Nonweiler, T. R. F., 1959, "Aerodynamic Problems of Manned Space Vehicles", Journal of the Royal Aeronautical Society, Vol. 63, Sept, pp. 521-528.
- Reller Jr., J. O., 1957, "Heat Transfer to Blunt Nose Shapes with Laminar Boundary Layers at High Supersonic Speeds", NACA RM-A57FO3a.
- Santos, W. F. N., 2003, "Aerodynamic Heating on Blunt Nose Shapes in Rarefied Hypersonic Flow", Proceedings of the 17th International Congress of Mechanical Engineering COBEM 2003, 10-14 Nov, São Paulo, SP, Brazil.
- Santos, W. F. N., 2004, "Surface Temperature Effects in Low-Density Flow over Flat-Nose Bodies at Hypersonic Speed. Part III: Shock Wave Structure", Proceedings of the 10th Brazilian Congress of Thermal Sciences and Engineering ENCIT 2004, 29 Nov – 3 Dec, Rio de Janeiro, RJ, Brazil.
- Santos, W. F. N., 2005a, "Gas-Surface Impact on Flowfield Structure of Low-Density Hypersonic Flow over Flat-Nose Bodies", Proceedings of the 18th International Congress of Mechanical Engineering COBEM 2005, 6-11 Nov, Ouro Preto, MG, Brazil.
- Santos, W. F. N., 2005b, "Simulation of Round Leading Edge Aerothermodynamics", Proceedings of the 18th International Congress of Mechanical Engineering COBEM 2005, 6-11 Nov, Ouro Preto, MG, Brazil.
- Santos, W. F. N., 2006, "A Numerical Study of the Compressibility Effect on Flowfield Structure of Blunt Bodies in Low-Density Flow", Proceedings of the IV National Congress of Mechanical Engineering CONEM 2006, 22-25 Agust, Recife, PE, Brazil (submitted).